Peroxidase activity was determined by following the oxidation of guaiacol for 1 min at 470 nm and was standardized by total protein content as previously described[36].

Bioassay with *P. syringae* pv. *tomato* DC3000

Fifteen replicates of each line were challenged by infiltration of three leaves with 10^4 colony-forming units per ml ($D_{600} = 0.002$) after 3 weeks of plant growth. After 5 days, leaf discs were removed, ground and plated on KB medium to determine the concentration of bacteria.

Received 18 February; accepted 18 March 2003; doi:10.1038/nature01588.

1. Grant, M. R. *et al.* Independent deletions of a pathogen-resistance gene in *Brassica* and *Arabidopsis*. *Proc. Natl Acad. Sci. USA* **87,** 15843–15848 (1998).
2. Caicedo, A. L., Schaal, B. A. & Kunkel, B. N. Diversity and molecular evolution of the *RPS2* resistance gene in *Arabidopsis thaliana*. *Proc. Natl Acad. Sci. USA* **96,** 302–306 (1999).
3. Stahl, E. A., Dwyer, G., Mauricio, R., Kreitman, M. & Bergelson, J. Dynamics of disease resistance polymorphism at the *Rpm1* locus of *Arabidopsis*. *Nature* **400,** 667–671 (1999).
4. Tian, D., Araki, H., Stahl, E., Bergelson, J. & Kreitman, M. Signature of balancing selection in *Arabidopsis*. *Proc. Natl Acad. Sci. USA* **99,** 11525–11530 (2002).
5. Mauricio, R., Korves, T., Stahl, E. A., Kreitman, M. & Bergelson, J. Natural selection for polymorphism in the disease resistance gene *RPS2* of *Arabidopsis*. *Genetics* **163,** 735–746 (2003).
6. Simms, E. L. & Rausher, M. D. Costs and benefits of plant resistance to herbivory. *Am. Nat.* **130,** 570–581 (1987).
7. Bergelson, J., Dwyer, G. & Emerson, J. J. Models and data on plant–enemy coevolution. *Annu. Rev. Genet.* **35,** 469–499 (2001).
8. Boyes, D. C., Nam, J. & Dangl, J. L. The *Arabidopsis thaliana RPM1* disease resistance gene product is a peripheral plasma membrane protein that is degraded coincident with the hypersensitive response. *Proc. Natl Acad. Sci. USA* **95,** 15849–15854 (1998).
9. Bisgrove, S. R., Simonich, M. T., Smith, N. M., Sattler, A. & Innes, R. W. A disease resistance gene in *Arabidopsis* with specificity for two different pathogen avirulence genes. *Plant Cell* **6,** 927–933 (1994).
10. Grant, M. R. *et al.* Structure of the Arabidopsis *RPM1* gene enabling dual specificity disease resistance. *Science* **269,** 843–846 (1995).
11. Redei, G. P. *Arabidopsis* as a genetic tool. *Annu. Rev. Genet.* **9,** 111–127 (1986).
12. Ow, D. W. & Medberry, S. L. Genome manipulation through site-specific recombination. *Crit. Rev. Plant Sci.* **14,** 239–261 (1995).
13. Howe, C. *Gene Cloning and Manipulation* (Cambridge Univ. Press, Cambridge, 1995).
14. Whalen, M. C., Innes, R. W., Bent, A. F. & Staskawicz, B. J. Identification of *Pseudomonas syringae* pathogens of *Arabidopsis* and a bacterial locus determining avirulence on both *Arabidopsis* and soybean. *Plant Cell* **3,** 49–59 (1991).
15. Mackey, D., Holt, B. F., Wiig, A. & Dangl, J. L. RIN4 interacts with *Pseudomonas syringae* Type III effector molecules and is required for RPM1-mediated resistance in *Arabidopsis*. *Cell* **108,** 743–754 (2002).
16. Jorgensen, J. H. & Jensen, H. P. Effect of 'unnecessary' powdery mildew resistance genes on agronomic properties of spring barley. *Norsk Landbruksforsking. Suppl.* **9,** 125–130 (1990).
17. Brown, J. K. M. Yield penalties of disease resistance in crops. *Curr. Opin. Plant Biol.* **5,** 1–6 (2002).
18. Rausher, M. D. Co-evolution and plant resistance to natural enemies. *Nature* **411,** 857–864 (2001).
19. Stuiver, M. H. & Custers, J. H. H. V. Engineering disease resistance in plants. *Nature* **411,** 865–868 (2001).
20. Bergelson, J. & Purrington, C. B. Surveying patterns in the cost of resistance in plants. *Am. Nat.* **148,** 536–558 (1996).
21. Wang, Z.-W., Yamanouchi, U., Katayose, Y., Sasaki, T. & Yano, M. Expression of the *Pib* rice-blast-resistance gene family is up-regulated by environmental conditions favouring infection and by chemical signals that trigger secondary plant defences. *Plant Mol. Biol.* **47,** 653–661 (2001).
22. Oldroyd, G. E. D. & Staskawicz, B. J. Genetically engineered broad-spectrum disease resistance in tomato. *Proc. Natl Acad. Sci. USA* **95,** 10300–10305 (1998).
23. Tang, X. *et al.* Overexpression of *Pto* activates defense responses and confers broad resistance. *Plant Cell* **11,** 15–29 (1999).
24. Mindrinos, M., Katagiri, F., Yu, G. & Ausubel, F. M. The *A. thaliana* disease resistance gene RPS2 encodes a protein containing a nucleotide-binding site and leucine-rich repeats. *Cell* **78,** 1089–1099 (1994).
25. Tao, Y., Yuan, F., Leister, R. T., Ausubel, F. M. & Katagiri, F. Mutational analysis of the *Arabidopsis* nucleotide binding site-leucine-rich repeat resistance gene RPS2. *Plant Cell* **12,** 2541–2554 (2000).
26. Holt, B. J. *et al.* An evolutionarily conserved mediator of plant disease resistance gene function is required for normal *Arabidopsis* development. *Dev. Cell* **2,** 807–817 (2002).
27. van der Biezen, E. A. & Jones, J. D. G. Plant disease resistance proteins and the gene for gene concept. *Trends Biochem. Sci.* **23,** 454–456 (1998).
28. Dangl, J. L. & Jones, J. D. G. Plant pathogens and integrated defence responses to infection. *Nature* **411,** 826–832 (2001).
29. Mackey, D., Belkhadir, Y., Alonso, J. M., Ecker, J. R. & Dangl, J. L. *Arabidopsis* RIN4 is a target of the Type III virulence effector AvrRpt2 and modulates RPS2-mediated resistance. *Cell* **112,** 379–389 (2003).
30. Gillespie, J. H. Natural selection for resistance to epidemics. *Ecology* **56,** 493–495 (1975).
31. Jakob, K. *et al. Pseudomonas viridiflava* and *P. syringae*—natural pathogens of *Arabidopsis thaliana*. *Mol. Plant–Microbe Interact.* **15,** 1195–1203 (2002).
32. Heid, C. A., Stevens, J., Livak, K. J. & Williams, P. M. Real time quantitative PCR. *Genome Res.* **6,** 986–994 (1996).
33. Klement, Z. Rapid detection of the pathogenicity of phytopathogenic Pseudomonads. *Nature* **199,** 299–300 (1963).
34. Moore, E. R. B. *et al.* The determination and comparison of the 16S rRNA gene sequences of species of the genus *Pseudomonas* (sensu stricto) and estimation of the natural intrageneric relationships. *Syst. Appl. Microbiol.* **19,** 478–492 (1996).
35. Dewdney, J. *et al.* Three unique mutants of *Arabidopsis* identify *eds* loci required for limiting growth of a biotrophic fungal pathogen. *Plant J.* **24,** 205–218 (2000).
36. Traw, M. B., Kim, J., Enright, S., Cipollini, D. F. & Bergelson, J. Negative cross-talk between the salicylate and jasmonate-mediated pathways in the Wassilewskija ecotype of *Arabidopsis thaliana*. *Mol. Ecol.* (in the press).

Acknowledgements We thank J. Dangl for feedback, and members of the Department of Ecology and Evolution for assistance in the field. This research was supported by NIH grants to J.B.

Competing interests statement The authors declare that they have no competing financial interests.

Correspondence and requests for materials should be addressed to J.B. (jbergels@midway.uchicago.edu).

Non-classical receptive field mediates switch in a sensory neuron's frequency tuning

Maurice J. Chacron*†, Brent Doiron*†, Leonard Maler†, André Longtin* & Joseph Bastian‡

** Physics Department, University of Ottawa, Ottawa, Ontario, Canada K1N 6N5*
† Department of Cellular and Molecular Medicine, University of Ottawa, Ottawa, Ontario, Canada K1H 8M5
‡ Department of Zoology, University of Oklahoma, Norman, Oklahoma 73019, USA

Animals have developed stereotyped communication calls to which specific sensory neurons are well tuned[1,2]. These communication calls must be discriminated from environmental signals such as those produced by prey. Sensory systems might have evolved neural circuitry to encode both categories. In weakly electric fish, prey and communication signals differ in their spatial extent and frequency content[3,4]. Here we show that stimuli of different spatial extents mimicking prey and communication signals cause a switch in the frequency tuning and spike-timing precision of electrosensory pyramidal neurons, resulting in the selective and optimal encoding of both stimulus categories. As in other sensory systems[5], pyramidal neurons respond only to stimuli located within a restricted region of space known as the classical receptive field (CRF)[6]. In some systems, stimulation outside the CRF but within a non-classical receptive field (nCRF) can modulate the neural response to CRF stimulation even though nCRF stimulation alone fails to elicit responses[7,8]. We show that pyramidal neurons possess a nCRF and that it can modulate the response to CRF stimuli to induce this neurobiological switch in frequency tuning.

The complex statistical structure of many naturalistic visual[9] and auditory[10] stimuli makes our interpretation of neural responses to these stimuli difficult and often prevents clearcut correlations of the responses with behaviour. Weakly electric fish offer a simple system for studying the differential encoding of natural stimuli because there is a clear spatiotemporal distinction between prey and communication stimuli. Amplitude modulations (AMs) of the electric fish's self-generated electric organ discharge (EOD) contain information relevant to both types of stimulus[11]. Epidermal electroreceptors encode these AMs precisely[12] and provide synaptic input[13] to pyramidal neurons of the electrosensory lateral line lobe (ELL), whose antagonistic centre–surround CRF structure[6] resembles that of visual neurons[5]. Relative motion of the fish near prey during feeding produces low-frequency (less than 10 Hz) spatially localized AMs[3]. However, communication signals from conspecifics produce high-frequency (more than 50 Hz) spatially diffuse AMs[4].

To provide naturalistic stimuli that mimic prey and communication signals, we used two stimulation geometries (see Methods). Local stimulus geometry provides AMs whose spatial extent is similar to that produced by prey, while global stimulus geometry produces spatially diffuse AMs similar to communication signals

(Fig. 1a, b). We investigated the frequency response properties of ELL pyramidal neurons by constructing EOD AM frequency tuning curves. Changing the stimulus geometry from local to global causes a shift in response preference from low to high frequencies (Fig. 1c; compare blue with red). We quantified this shift by computing the frequencies associated with the maximum vector strength (see Methods) under each stimulus geometry. These averaged 4.67 ± 2.73 Hz and 53.33 ± 16.52 Hz, respectively (mean change of 48.66 Hz, $P = 0.0004$, pairwise t-test, $n = 7$). Plots of the stimulus–spike train coherence obtained from random AM stimulation (see Methods) showed a qualitatively similar effect (Fig. 1d; compare blue with red). The average coherence values C_{low} between 0 and 20 Hz and C_{high} between 40 and 60 Hz were also computed. With global stimulus geometry, high-frequency coherence was significantly greater than low-frequency coherence ($P < 10^{-3}$, t-test, $n = 17$), but with local stimulus geometry the opposite frequency preference was seen ($P < 10^{-3}$, t-test, $n = 17$). Firing rates did not change as we went from local (23.12 ± 10.86 spikes s^{-1}) to global (23.24 ± 11.82 spikes s^{-1}) geometry ($P = 0.9$, pairwise t-test, $n = 17$). This confirms that ELL pyramidal neurons behave as low-pass filters when stimulated locally, whereas they exhibit high-pass characteristics when stimulated globally.

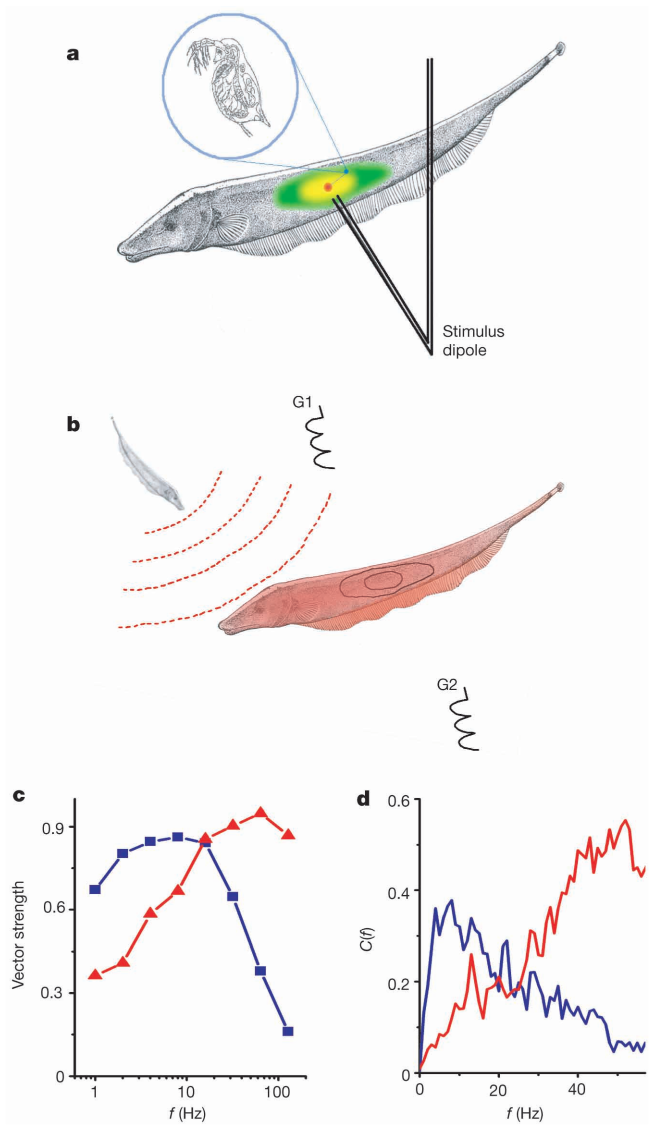

Figure 1 ELL pyramidal neurons display differential frequency tuning to local and global stimulation geometries. **a**, Local stimulation geometry. A small stimulus dipole (2-mm tip spacing) was positioned 2–3 mm lateral to the fish and delivered AMs of the animal's own electric organ discharge. These AMs were spatially localized (red circle) over only a fraction of the CRF centre (yellow ellipse). They did not stimulate the surround (green ellipse) or the nCRF lying outside the surround. The electric image was spatially similar to that produced by a prey (*Daphnia*, blue circle) as the fish swims by. **b**, Global stimulation geometry. Two silver–silver-chloride electrodes (G1 and G2) were placed about 19 cm lateral to each side of the animal. Global AMs (red) stimulate the entire body surface including the CRF centre and surround and also any putative nCRF, and are spatially similar to those produced by communication stimuli. In addition, the ipsilateral and contralateral body surfaces receive stimuli in antiphase. **c**, Tuning curves (vector strength plotted against frequency) for single-unit responses from ELL pyramidal neurons obtained under local (blue) and global (red) stimulus geometries. The vector strength under local stimulus geometry is maximal for frequencies of less than 10 Hz. However, it is maximal for frequencies of about 100 Hz under global stimulus geometry. **d**, Coherence curve (see Methods) obtained under local (blue) and global (red) stimulus geometries. The curves are qualitatively similar to the tuning curves obtained in **c**.

We used information theoretic measures[14,15] (see Methods) to quantify the consequences for stimulus encoding of this shift in temporal frequency tuning. We compared results obtained with locally and globally applied low-frequency (0–20-Hz) and high-frequency (40–60-Hz) random AMs. These results are summarized in Table 1. High-frequency global stimuli (communication-like) were encoded much better (about 200%) than high-frequency local stimuli. Moreover, low-frequency local stimuli (prey-like) were encoded much better (about 100%) than low-frequency global stimuli. These results demonstrate that pyramidal neurons show improved stimulus encoding when the combination of temporal frequency content and spatial stimulus characteristics closely mimic those of natural stimuli.

The higher mutual information rates, indicating an increased signal-to-noise ratio, obtained with high-frequency global stimuli as compared with high-frequency local stimuli indicate a possible dependence of spike train variability on the spatial extent of the stimulus. Neurons can display low trial-to-trial variability to repeated stimuli both *in vitro*[16] and *in vivo*[17]. Using 'frozen noise' (see Methods), we explored the reliability of spike timing displayed by ELL pyramidal neurons. Results show high trial-to-trial variability under local stimulus geometry (Fig. 2a) and low trial-to-trial variability under global stimulus geometry (Fig. 2b). The average reliability of spike timing, measured as the fraction of spikes occurring reproducibly during high-frequency 'events'[16], increased from 0.16 ± 0.17 under local stimulation to 0.72 ± 0.12 with global stimulation ($P = 0.004$, pairwise t-test, $n = 7$). The mean spike time precision (average standard deviation of spike times within 'events'[16]) decreased from 1.44 ± 0.16 ms under local stimulation to 1.08 ± 0.23 ms with global stimulation ($P = 0.009$, pairwise t-test, $n = 7$). Pyramidal neurons display high reliability and high spike timing precision to stimuli mimicking the frequency content of communication signals, but only when the stimulus is presented globally. Such timing precision does not occur for low-frequency stimuli (data not shown), presumably because accurate encoding of low-frequency stimuli does not require such high temporal precision.

Table 1 **Summary of results with different information-theoretic measures**

	Local	Global
High frequency	$\gamma = 0.08 \pm 0.08$ $I = 0.29 \pm 0.28$	$\gamma = 0.25 \pm 0.17$ $I = 1.14 \pm 0.52$
Low frequency	$\gamma = 0.26 \pm 0.11$ $I = 0.74 \pm 0.33$	$\gamma = 0.15 \pm 0.12$ $I = 0.36 \pm 0.20$
Statistical significance	$P_\gamma = 0.0031$ ($n = 12$) $P_I = 0.0035$ ($n = 12$)	$P_\gamma = 0.0015$ ($n = 11$) $P_I = 0.0014$ ($n = 11$)

The coding fraction, γ, is the fraction of the stimulus waveform correctly estimated by the neuron; the mutual information rate, I, in bits per spike gives the amount of information transmitted by the neuron by each spike. P_γ and P_I are the respective P values obtained from a pairwise t-test comparing the γ and I values obtained with high-frequency (40–60-Hz) stimuli with those obtained with low-frequency (0–20-Hz) stimuli.

Anatomical studies[18,19] predict that local and global stimulation will activate different constellations of synaptic inputs to ELL pyramidal neurons. If these differing synaptic inputs cause the shift in frequency tuning, this should be reflected in the cell's membrane potential. We recorded intracellularly from pyramidal neurons to test this hypothesis. Figure 2 shows the membrane potential response under local (Fig. 2c) and global (Fig. 2d) stimulation geometry with random AM stimulation. The membrane potential response (black) does not track the higher-frequency components of the stimulus (blue) during local stimulation but does so during global stimulation. We emphasize this point by computing the coherence between the membrane potential response with spikes removed (green) (see Methods) and the stimulus (Fig. 2e, f). For local stimulus geometry, C_{low} was significantly greater than C_{high} ($P = 0.024$, t-test, $n = 6$) whereas the opposite was true for global stimulus geometry ($P = 0.012$, t-test, $n = 6$). These results show that the change in frequency tuning is seen in the membrane potential response itself and thus probably originates from differing synaptic inputs under local and global stimulus geometries.

We have previously mapped the antagonistic centre–surround CRF organization of ELL pyramidal neurons[6]. Local stimuli affect only a fraction of the CRF centre (Fig. 1a) whereas global stimuli influence the entire CRF as well as the nCRF (Fig. 1b). In the visual system, the nCRF is known to modulate CRF centre responses[7,8]. To test for the presence of nCRF effects and their possible role in pyramidal neuron frequency tuning shifts, we performed partition experiments (see Methods) illustrated in Fig. 3a. The thin rubber partition electrically isolated the fish's head region from its trunk region, allowing each to be independently stimulated. We recorded from pyramidal neurons whose CRF centre was sufficiently distant from the partition to ensure that the CRF was entirely within the trunk region. Thus, stimuli applied to the head region influenced the responsiveness of the recorded cell only through the nCRF. Local stimulation of the CRF centre alone with 0–60 Hz random AMs produced results identical to those obtained under local stimulus geometry without a partition (compare Figs 1d and 3b, blue). We then paired the local CRF centre stimulation with in-phase global stimulation of the head chamber (Fig. 3b, red). Simultaneous stimulation of the nCRF decreased the cell's response to low frequencies only. The measure of low-frequency coherence, C_{low}, was significantly decreased ($P < 10^{-3}$, pairwise t-test, $n = 15$). This decrease is similar to that seen in the transition from local to global geometries. However, nCRF stimulation phase-shifted by 180° relative to the CRF had no effect on coherence (Fig. 3b, green); there was

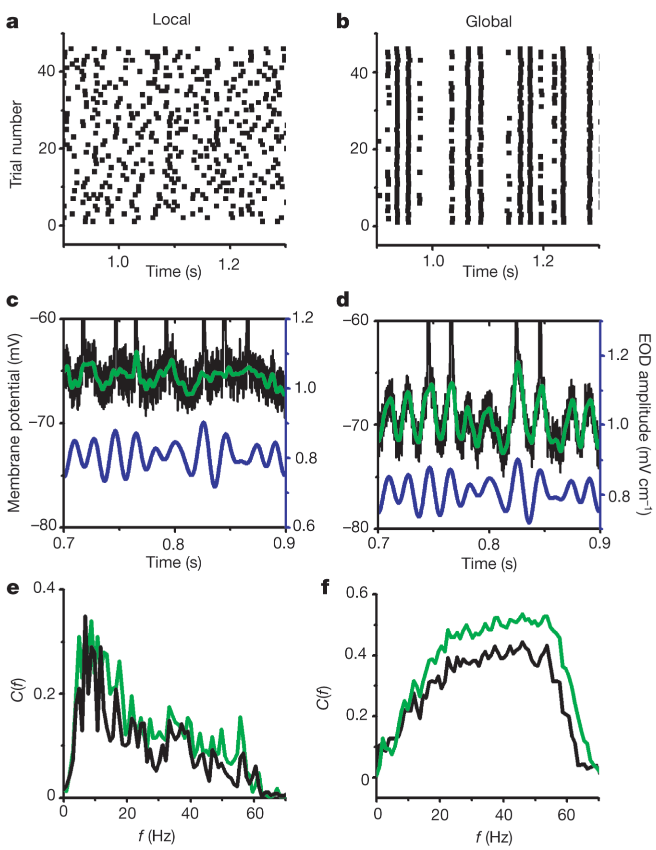

Figure 2 Spike timing reliability and precision under local and global stimulation geometries. **a**, Raster plot showing responses to short subsets of 2-s epochs of frozen 40–60-Hz random AMs presented locally. **b**, As in **a**, but the stimuli were presented with global stimulus geometry. **c**, Intracellularly recorded membrane potential response V_m (black trace) from a pyramidal cell under local 0–60-Hz random AM stimulation. The ~72-mV-high spikes are truncated. The green trace shows V_m after spikes had been removed and replaced with the means of V_m immediately before and after each spike, then low-pass filtered (200-Hz cut-off, eighth-order Butterworth). The blue trace shows the time course of EOD AMs measured within the centre of the cell's receptive field and low-pass filtered with the same filter parameters. The EOD AM was shifted by ~7 ms to compensate for axonal and synaptic delays. Comparison of the green and blue traces shows that V_m fails to follow the high-frequency components of the stimulus. **d**, V_m from the same cell but with global stimulus geometry. **e**, Coherence between stimulus and membrane potential response with spikes removed (green) and coherence between stimulus and spike train (black) under local 0–60-Hz random AM stimulation. **f**, As in **e**, but with global stimulus geometry.

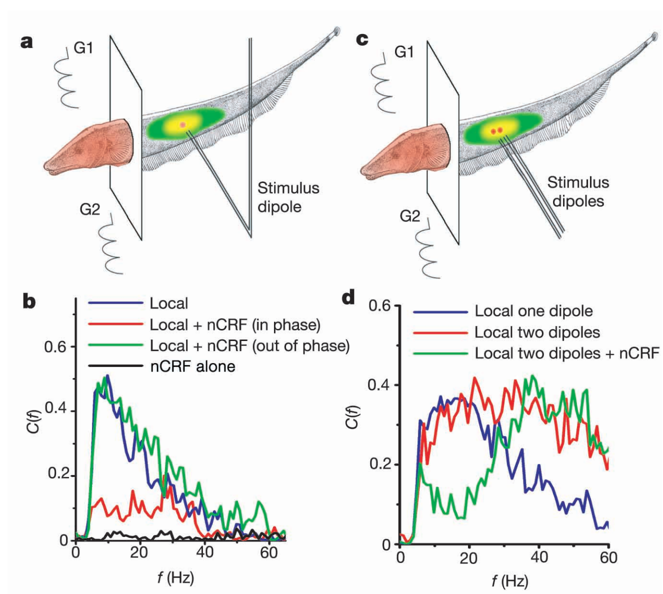

Figure 3 The nCRF mediates pyramidal neuron frequency tuning. **a**, Partition experiments. The animal's head was electrically isolated from the trunk by a thin rubber partition so that stimuli could be presented to the head and trunk regions independently (see Methods). **b**, Effects of pairing local trunk stimulation with global stimulation of the head chamber. Local stimulation of the CRF centre alone produces high coherence at low frequencies and low coherence at high frequencies (blue), as in Fig. 1c. Pairing local stimulation with in-phase head-chamber (nCRF) stimulation decreased low-frequency responsiveness (red); 180° phase-shifting of the nCRF stimulus relative to the CRF centre stimulus resulted in no loss of low-frequency coherence (green). nCRF stimulation alone was ineffective (black). **c**, Increased spatial saturation of the CRF centre was accomplished with two stimulus dipoles. **d**, Stimulation of the CRF centre by two dipoles (red trace) preferentially increased the cell's response to high frequencies over stimulation with one dipole (blue trace). The addition of nCRF stimulation attenuated low-frequency responsiveness (green).

no significant change in C_{low} and C_{high} ($P = 0.36$ and 0.16 respectively, pairwise t-tests, $n = 15$). Stimulation of the head region alone was ineffective in driving the recorded cell (Fig. 3b, black).

The cells' firing rates decreased by 3.9 and 2.1 spikes s^{-1} on average under in-phase and out-of-phase paired stimulation of CRF plus nCRF, respectively ($P = 0.003/0.001$, pairwise t-tests, $n = 15$). Because, in each case, the neurons received the same amount of primary afferent excitation by means of the CRF centre, the cells must be inhibited by nCRF stimulation. Furthermore, because the nCRF stimulus must be in phase with the CRF stimulus to decrease a neuron's response to low frequencies, the inhibition must act on a moderately fast timescale. Paired stimulation of the CRF centre plus the nCRF in phase did not on average alter high-frequency response because C_{high} did not change significantly with in-phase nCRF stimulation ($P = 0.58$, pairwise t-test, $n = 15$).

Either global stimulus geometry or paired stimulation of the nCRF plus the CRF centre in the partition experiment reduced low-frequency coherence. However, only global stimulation (no partition) resulted in an improvement in high-frequency coherence. Global geometry not only results in nCRF stimulation but also ensures that the entire CRF centre is stimulated (spatial saturation). Hence, the complete shift in frequency tuning seen with the transition from local to global geometry (Fig. 1c, d) might require both stimulation of the nCRF as well as spatial saturation of the CRF centre. To test the latter hypothesis we repeated the partition experiment but increased the CRF centre area influenced by the local stimulus by adding a second dipole (Fig. 3c; see Methods). As shown in Fig. 3d (compare blue and red), addition of the second dipole increased C_{high} by about 70% ($P = 0.0027$, pairwise t-test, $n = 7$). Thus, combining saturation of the CRF centre with in-phase nCRF stimulation is sufficient to induce both the increase in the cell's high-frequency response and the decrease in its low-frequency response (Fig. 3d, green) just as in the normal transition from local to global geometry. Stimulation of the CRF surround did not alter the frequency tuning to stimulation of the CRF centre (data not shown).

We have demonstrated that ELL pyramidal neurons can switch their tuning properties on the basis of the spatial extent of a stimulus. Specifically, pyramidal neurons responded maximally to temporal frequencies below 10 Hz under spatially local stimulation and to frequencies over 50 Hz under spatially global stimulation. These responses are well matched to the observed temporal frequency content of prey[3] and communication[4] stimuli, respectively. Maximum information transfer was obtained when the stimulus matched the spatiotemporal content of prey and communication stimuli. In particular, high information transfer was obtained for high-frequency global stimuli. This differs from previous results[6,12] that showed poor information transfer under a global-like geometry. However, both previous studies used mainly low-frequency stimuli, to which pyramidal neurons respond poorly under global stimulation.

Intracellular recordings revealed that a change in synaptic input was probably responsible for the change in frequency tuning. The reduced response to low frequencies under global stimulation is due primarily to nCRF stimulation, probably acting through inhibition because a decrease in firing rate was observed. This decreased response is thus unlikely to occur with global yet spatially heterogeneous environmental stimuli such as those caused by a root mass[20], because it requires spatially homogeneous communication-like signals. ELL pyramidal neurons receive inhibition from several sources[18,19]. Inhibition is known to modulate neural frequency tuning[21] and can lead to oscillations and synchrony in a neural population[22]. We have recently shown that ELL pyramidal neurons displayed inhibition-mediated oscillatory dynamics under global stimulation but not under local stimulation[23]. The emergence of this oscillation can sometimes accompany the shift in frequency response found here, but is not required to induce it (data not shown).

Our study shows that the structure of the receptive field of ELL pyramidal neurons is well adapted to categorical coding of their natural stimulus environment. This is achieved through the differential spatial extent of prey and communication stimuli that will differentially activate the structure of the receptive field of pyramidal neurons. Prey-like stimuli activate only a fraction of the CRF centre, whereas communication stimuli spatially saturate the CRF centre and also activate the nCRF, thus producing different synaptic input from that for prey stimuli. This neurobiological switch in synaptic input allows pyramidal neurons to encode both prey and communication stimuli optimally. □

Methods

Stimulation and recording

The experimental protocol has been described previously[6]. The stimuli consisted of sinusoidal and band-limited random AMs of an animal's own EOD presented with local or global geometry. When two local stimulus dipoles were used, the same stimulus waveform was fed to independent stimulus isolation units, each of which drove one dipole. Recordings were limited to E-type pyramidal neurons of the centrolateral and lateral segments[24,25], which are important for processing both high-frequency communication signals[26,27] and prey stimuli[6]. The centromedial ELL segment, required for the jamming avoidance response evoked by low-frequency global stimuli[28], is not considered here.

Extracellular single-unit recordings were made with metal-filled microelectrodes, and intracellular recordings were made with 40–100-MΩ KCl-filled micropipettes. Standard methods of preamplification were used and data were acquired with Cambridge Electronic Design 1401plus hardware and SpikeII software. All surgical procedures were performed in accordance with the University of Oklahoma animal care and use guidelines.

Data analysis

Spike trains during sinusoidal AM stimulation were accumulated as cycle histograms and the response was quantified by using the vector strength[6,29], which measures the degree of phase locking and ranges between 0 (no phase locking) and 1 (perfect phase locking).

Responses to random AMs were analysed by computing the coherence, $C(f)$, between the spike train and stimulus, where $C(f) = |P_{sx}(f)|^2/[P_{ss}(f)P_{xx}(f)]$. $P_{ss}(f)$ and $P_{xx}(f)$ are the power spectra of the stimulus and spike train respectively, and $P_{sx}(f)$ is the cross-spectrum between the stimulus and the spike train. $C(f)$ ranges from 0 to 1 and indicates the strength of the response to the stimulus at a frequency f. Animals often displayed electrocommunication responses to random AMs, but only when these were applied globally (data not shown), indicating that these stimuli are good communication signal mimics.

We used the 'frozen noise' technique to examine trial-to-trial variability: the same random AM (40–60 Hz, duration 2 s) was delivered at least 30 times. We computed the reliability and precision measures from post-stimulus time histograms (binwidth 3 ms) as described previously[16].

Information theoretic measures

A lower bound on the mutual information rate (in bits s^{-1}) is given in refs 14 and 30:

$$I = -\int_{f_{low}}^{f_{high}} df \log_2[1 - C(f)]$$

where f_{low} and f_{high} define the bandwidth of the stimulus. We obtained the mutual information rate in bits per spike by dividing I by the cell's mean firing rate during stimulation.

We performed linear stimulus reconstruction[14,30] as reported previously[6]. Note that this provides an absolute lower bound on information transmission[30]. The quality of the reconstruction was quantified by the coding fraction, γ, which is a number between 0 and 1, with $\gamma = 1$ implying perfect reconstruction.

Partition experiment

The animal's head was electrically isolated from the trunk by a thin rubber partition so that stimuli could be presented to the head and trunk regions independently. The partition decreased the normal EOD amplitude in the head region because it partly blocked EOD current flow. To compensate for this a continuous unmodulated EOD mimic signal was delivered to the head region between a single electrode in the dorsal musculature and electrodes lateral to either side of the fish. This restored the EOD amplitude in the head region to values measured with the partition short-circuited. C_{low} and C_{high} values with the partition in place for local stimulation were not statistically different from those obtained without the partition ($P = 0.4359$ and $P = 0.95$ respectively, t-tests, $n = 15$).

Single electroreceptor afferents were recorded and stimulated with 4-Hz sinusoidal AMs to gauge the effectiveness of electrical isolation. Each afferent's responses to stimuli presented in the head and trunk regions were summarized as cycle histograms and quantified as vector strengths. The Rayleigh statistic[29] was also calculated to determine whether the cycle histogram showed statistically significant phase-locking to the AM. Receptor afferent receptive field positions ranged from 8 to 45 mm rostral or caudal to the partition. Stimulation of the receptor-containing region (1 mV cm^{-1} AM) resulted in a mean Rayleigh statistic of 758 ± 125, showing significant phase-locking. Stimuli applied to the region not containing the receptor resulted in a mean Rayleigh statistic of 0.928 ± 0.321. No receptor afferents recorded showed statistically significant phase-locking to the AM applied to the chamber not containing its receptive field.

The average distance between the partition and the CRF centre was 5.6 cm and was always greater than 4 cm. Using results reported previously[6], we estimated the maximal CRF dimensions as follows. Average CRF centre and surround areas were summed, then doubled. The maximum distance from the centre of the receptive field to the CRF boundary was then estimated as the radius of a circle having this area (2.4 cm). This conservative estimate is lower than 4 cm. Along with the lack of pyramidal-cell responses to stimulation of the head chamber alone, this indicates that it is very unlikely that the CRF surround extends past the partition.

Received 20 January; accepted 17 March 2003; doi:10.1038/nature01590.

1. Rieke, F., Bodnar, D. A. & Bialek, W. Naturalistic stimuli increase the rate and efficiency of information transmission by primary auditory afferents. *Proc. R. Soc. Lond. B* **262,** 259–265 (1995).
2. Machens, C. K. *et al.* Representation of acoustic communication signals by insect auditory neurons. *J. Neurosci.* **21,** 3215–3227 (2001).
3. Nelson, M. E. & MacIver, M. A. Prey capture in the weakly electric fish *Apteronotus leptorhynchus*: sensory acquisition strategies and electrosensory consequences. *J. Exp. Biol.* **202,** 1195–1203 (1999).
4. Zupanc, G. K. H. & Maler, L. Evoked chirping in the weakly electric fish *Apteronotus leptorhynchus*: a quantitative biophysical analysis. *Can. J. Zool.* **71,** 2301–2310 (1993).
5. Hubel, D. H. & Wiesel, T. N. Receptive fields, binocular interaction and functional architecture in the cat's visual cortex. *J. Physiol. (Lond.)* **160,** 106–154 (1962).
6. Bastian, J., Chacron, M. J. & Maler, L. Receptive field organization determines pyramidal cell stimulus-encoding capability and spatial stimulus selectivity. *J. Neurosci.* **22,** 4577–4590 (2002).
7. Sillito, A. M., Grieve, K. L., Jones, H. E., Cudeiro, J. & Davis, J. Visual cortical mechanisms detecting focal orientation discontinuities. *Nature* **378,** 492–496 (1995).
8. Vinje, W. & Gallant, J. L. Sparse Coding and decorrelation in primary visual cortex during natural vision. *Science* **287,** 1273–1276 (2000).
9. Simoncelli, E. P. & Olshausen, B. A. Natural image statistics and neural representation. *Annu. Rev. Neurosci.* **24,** 1193–1216 (2001).
10. Voss, R. F. & Clarke, J. '1/*f* noise' in music: music from 1/*f* noise. *J. Acoust. Soc. Am.* **63,** 258–263 (1978).
11. Bastian, J. Electrolocation. I. How the electroreceptors of *Apteronotus albifrons* code for moving objects and other electrical stimuli. *J. Comp. Physiol. A* **144,** 465–479 (1981).
12. Gabbiani, F., Metzner, W., Wessel, R. & Koch, C. From stimulus encoding to feature extraction in weakly electric fish. *Nature* **384,** 564–567 (1996).
13. Maler, L., Sas, E. K. & Rogers, J. The cytology of the posterior lateral line lobe of high frequency weakly electric fish (*Gymnotoidei*): Dendritic differentiation and synaptic specificity in a simple cortex. *J. Comp. Neurol.* **195,** 87–139 (1981).
14. Rieke, F., Warland, D., de Ruyter van Steveninck, R. R. & Bialek, W. *Spikes: Exploring the Neural Code* (MIT, Cambridge, Massachusetts, 1996).
15. Borst, A. & Theunissen, F. Information theory and neural coding. *Nature Neurosci.* **2,** 947–957 (1999).
16. Mainen, Z. F. & Sejnowski, T. J. Reliability of spike timing in neocortical neurons. *Science* **268,** 1503–1506 (1995).
17. de Ruyter van Steveninck, R. R., Lewen, G. D., Strong, S. P., Koberle, R. & Bialek, W. Reproducibility and variability in neural spike trains. *Science* **275,** 1805–1808 (1997).
18. Maler, L. & Mugnaini, E. Correlating gamma-aminobutyric acidergic circuits and sensory function in the electrosensory lateral line lobe of a gymnotiform fish. *J. Comp. Neurol.* **345,** 224–252 (1994).
19. Berman, N. J. & Maler, L. Neural architecture of the electrosensory lateral line lobe: Adaptations for coincidence detection, a sensory searchlight and frequency-dependent adaptive filtering. *J. Exp. Biol.* **202,** 1243–1253 (1999).
20. Crampton, W. G. R. Electric signal design and habitat preferences in a species rich assembly of gymnotiform fishes from the upper Amazon basin. *Anais Acad. Bras. Cienc.* **70,** 805–847 (1998).
21. Zhang, H., Xu, J. & Feng, A. S. Effects of GABA-mediated inhibition on direction-dependent frequency tuning in the frog inferior colliculus. *J. Comp. Physiol.* **184,** 85–98 (1999).
22. Macleod, K. & Laurent, G. Distinct mechanisms for synchronization and temporal patterning of odor-encoding neural assemblies. *Science* **274,** 976–979 (1996).
23. Doiron, B., Chacron, M. J., Maler, L., Longtin, A. & Bastian, J. Inhibitory feedback required for network burst responses to communication but not prey stimuli. *Nature* **421,** 539–543 (2003).
24. Carr, C. E., Maler, L. & Sas, E. Peripheral organization and central projections of the electrosensory organs in gymnotiform fish. *J. Comp. Neurol.* **211,** 139–153 (1982).
25. Heiligenberg, W. & Dye, J. Labelling of electrosensory afferents in a gymnotid fish by intracellular injection of HRP: The mystery of multiple maps. *J. Comp. Physiol. A* **148,** 287–296 (1982).
26. Metzner, W. & Heiligenberg, W. The coding of signals in the electric communication of the gymnotiform fish *Eigenmannia*: From electroreceptors to neurons in the torus semicircularis of the midbrain. *J. Comp. Physiol. A* **169,** 135–150 (1991).
27. Metzner, W. & Juranek, J. A sensory brain map for each behavior? *Proc. Natl Acad. Sci. USA* **26,** 14798–14803 (1997).
28. Heiligenberg, W. *Neural Nets in Electric Fish* (MIT, Cambridge, Massachusetts, 1991).
29. Bastchelet, E. *Circular Statistics in Biology* (Academic, New York, 1981).
30. Gabbiani, F. Coding of time varying signals in spike trains of linear and half-wave rectifying neurons. *Network Comput. Neural Sys.* **7,** 61–85 (1996).

Acknowledgements We thank A.-M. Oswald, J. Lewis and B. Lindner for their reading the manuscript. This research was supported by NSERC (M.J.C., B.D., A.L.), CIHR (L.M., A.L.) and NIH (J.B.).

Competing interests statement The authors declare that they have no competing financial interests.

Correspondence and requests for materials should be addressed to M.J.C. (mchacron@physics.uottawa.ca).

The genome sequence of *Bacillus anthracis* Ames and comparison to closely related bacteria

Timothy D. Read*†, Scott N. Peterson*‡, Nicolas Tourasse§#, Les W. Baillie*†||, Ian T. Paulsen*¶, Karen E. Nelson*, Hervé Tettelin*, Derrick E. Fouts*, Jonathan A. Eisen*¶, Steven R. Gill*, Erik K. Holtzapple*, Ole Andreas Økstad§#, Erlendur Helgason§#, Jennifer Rilstone*, Martin Wu*, James F. Kolonay*, Maureen J. Beanan*, Robert J. Dodson*, Lauren M. Brinkac*, Michelle Gwinn*, Robert T. DeBoy*, Ramana Madpu*, Sean C. Daugherty*, A. Scott Durkin*, Daniel H. Haft*, William C. Nelson*, Jeremy D. Peterson*, Mihai Pop*, Hoda M. Khouri*, Diana Radune*, Jonathan L. Benton*, Yasmin Mahamoud*, Lingxia Jiang*, Ioana R. Hance*, Janice F. Weidman*, Kristi J. Berry*, Roger D. Plaut*, Alex M. Wolf*, Kisha L. Watkins*, William C. Nierman*, Alyson Hazen*, Robin Cline*, Caroline Redmond†, Joanne E. Thwaite†, Owen White*, Steven L. Salzberg*¶, Brendan Thomason☆, Arthur M. Friedlander, Theresa M. Koehler††, Philip C. Hanna☆, Anne-Brit Kolstø§# & Claire M. Fraser*‡‡§§**

* *The Institute for Genomic Research, 9712 Medical Center Drive, Rockville, Maryland 20850, USA*
† *Medical Biotechnology Center, University of Maryland Biotechnology Institute, Baltimore, Maryland 21201, USA*
‡ *Department of Biochemistry,* ‡‡ *Department of Microbiology and Tropical Medicine,* §§ *Department of Pharmacology, The George Washington University, Eye Street, Washington DC 20052, USA*
§ *School of Pharmacy, University of Oslo N-0316, Oslo, Norway*
|| *Defence Science Technology Laboratory, Porton Down, Salisbury SP4 0JQ, UK*
¶ *Johns Hopkins University, Charles and 34th Streets, Baltimore, Maryland 21218, USA*
# *The Biotechnology Center of Oslo, Oslo N-0317, Norway*
☆ *Department of Microbiology & Immunology, University of Michigan Medical School, Ann Arbor, Michigan 48109, USA*
** *US Army Medical Research Institute for Infectious Diseases, Frederick, Maryland 21702, USA*
†† *Department of Microbiology and Molecular Genetics, University of Texas–Houston Health Science Center Medical School, University of Texas, Houston, Texas 77225, USA*

Bacillus anthracis **is an endospore-forming bacterium that causes inhalational anthrax[1]. Key virulence genes are found on plasmids (circular, self-replicating double-stranded DNA molecules) pXO1 (ref. 2) and pXO2 (ref. 3). To identify additional genes that might contribute to virulence, we analysed the complete sequence of the chromosome of *B. anthracis* Ames (about 5.23 megabases). We found several chromosomally encoded proteins that may contribute to pathogenicity—including haemolysins, phospholipases and iron acquisition functions—and identified numerous surface proteins that might be important targets for vaccines and drugs. Almost all these putative chromosomal virulence and surface proteins have homologues in *Bacillus cereus*, highlighting the similarity of *B. anthracis* to near-neighbours that are not associated with anthrax[4]. By performing a comparative genome hybridization of 19 *B. cereus* and *Bacillus thuringiensis* strains against a *B. anthracis* DNA microarray, we confirmed the general similarity of chromosomal genes among this group of close relatives. However, we found that the gene sequences of pXO1 and pXO2 were more variable between strains, suggesting plasmid mobility in the group. The complete sequence of *B. anthracis* is a step towards a better understanding of anthrax pathogenesis.**

B. anthracis has become notorious as a bioweapon because of its tough, environmentally resistant endospore and its ability to cause lethal inhalational anthrax. During the course of the disease,